CONTINENTAL J. APPLIED SCIENCES
Hamza and Magami (2017) 12 (3): 12 – 28 DOI: 10.5281/zenodo.886898

Research Article

Transient hydromagnetic free convection flow of reactive viscous fluid in a vertical channel with Soret effect

M.M. Hamza and M.S. Magami
Department of Mathematics, Usmanu Danfodiyo University, Sokoto, P.M.B. 2346, Nigeria Email: hmbtamb@yahoo.com

Abstract

Unsteady/steady hydromagnetic natural convection heat and mass transfer flow characteristics of viscous reactive, incompressible and electrically conducting fluid in a vertical channel with Soret effect in the presence of uniform transverse magnetic field is studied. It is assumed that the chemical kinetics in the flow system is exothermic. The analytical expressions for the steady-state version of the problem has been derived for the temperature, concentration, velocity, skin friction, rate of heat transfer and rate of mass transfer using perturbation series method. The solutions for unsteady state temperature, concentration and velocity are obtained numerically using semi-implicit finite difference scheme. Numerical results are graphically discussed for various values of physical parameters embedded in the problem.

Keywords: natural convection, heat transfer, mass transfer, hydromagnetic, unsteady/steady flow, Soret effect.

Received: 25June 2017 Accepted: 02Sept. 2017

Introduction

Heat and mass transfer problems on natural convection flow in a vertical channel found applications in natural circulation in geothermal reservoir, packed bed reactors, sensible heat storage beds and beds of fossil fuels such as oil shale and coal which is fragmented in situ energy extraction Postelnicu (2004). In an attempt to study natural convection on heat and mass transfer flows, Soundalgekar and Warve (1977) studied unsteady natural convection flow past an infinite vertical plate with constant suction and mass transfer. In

ISSN: 1597 – 9928 Science and Education Development Inst., Nigeria

another article Soundalgekar and Ganesan (1981) investigated numerically unsteady natural convection flow and mass transfer on an isothermal vertical flat plate. Joshi (1988) analyzed unsteady effects in natural convection cooling of vertical parallel plates. Combined heat and mass transfer flow on natural convection between vertical parallel plates have been reported by Nelson and Wood (1989). Unsteady natural convection and mass transfer flow in a vertical channel have been studied by Yan and Lin (1990), and Lee (1999). Natural convection and mass transfer flow in a vertical channel in the presence of chemical reaction is important in the design of several equipment used in engineering systems. For instance in the design of nuclear reactors, thermal insulation, surface catalysis of chemical reaction, small domestic mobile winter oil heaters, and some types of radiators and hydronic heating systems. In chemical engineering and petroleum chemical industries the interaction between chemical reaction and natural convection occurs widely. Areas of such applications include tubular laboratory reactors, chemical vapor deposition systems, and the oxidation of solid materials in large containers, the synthesis of ceramic materials by a self-propagating reaction and many others. Natural convection flow driven by an exothermic reaction on a vertical surface embedded in porous media was studied by Minto *et al*. (1998). Campbell *et al*. (2007) conducted comparison of measured temperatures with those calculated numerically and analytically for an exothermic chemical reaction inside a spherical batch reactor with natural convection. They concluded that the transport of heat and mass transfer within the reactor is controlled by diffusion or natural convection. Recently Jha et al. (2011a, 2011b, 2012, and 2013) investigated unsteady natural convection flow of reactive viscous fluid in a vertical channel as well as vertical tube and the reaction is exothermic under Arrhenius kinetics, neglecting the consumption of the materials. In the other hand, Soret or thermal diffusion is important where more than one chemical species are present under a very large temperature gradients, such as chemical reactions, isotope separation and in mixture between gases with very light molecular weight such as hydrogen or helium and of medium molecular weight such as nitrogen or air. Dursunkaya and Worek (1992) considered the effects of Soret and Dufour in transient and steady natural convection from vertical channel. Tsai and Huang (2009) investigated numerically the effects of Soret and Dufour on heat and mass transfer from natural convection flow over a vertical porous medium with variable wall fluxes.

In the last seventy years, the interest in the study of flow of an electrically conducting fluid in a vertical channel has been growing rapidly. The interest in such problem stems from their important applications in engineering and industrial processes, such as MHD marine propulsion, electronic packages, microelectronic devices, thermal insulation, petroleum reservoirs, MHD stirring of molten metal, exothermic reaction in package reactors and magnetic-levitation casing. The Hartmann (1937) pioneering work on the

ISSN: 1597 – 9928 Science and Education Development Inst., Nigeria

investigation of hydromagnetic flow between two infinite parallel plates experimentally as well as theoretically is regarded as the origin of MHD channel flow. This investigation provided the fundamental knowledge for the development of many MHD devices such as MHD pumps, MHD generators, brakes, flow meters, plasma studies and geothermal energy extraction. In this direction, Emmanuel e*t al*. (2008) determined numerically the effects of Soret and Dufour on heat and mass transfer of a steady MHD convective and slip flow due to a rotating disk with viscous dissipation and ohmic heating. Recently Turkyilmazoglu and Pop (2012) reported the effects of Soret and heat source on unsteady radiative MHD free convection flow from an impulsively infinite vertical plate.

The present paper is committed to study unsteady as well as steady hydromagnetic flow of viscous reactive, incompressible and electrically conducting fluid between two infinite vertical parallel plates in the presence of a uniform transverse magnetic field with Soret effect. The features of the flow characteristics are analyzed by plotting graphs. The paper has been organized as follows. The mathematical formulation of the problem and the non-dimensional governing equations are established in section 2. The analytical solutions for steady state version of the problem are presented in section 3. In section 4 the semi-implicit finite difference technique for the complete form of the problem is implemented in time and space for the solution process. Numerical results and discussion are presented in section 5. The conclusions have been summarized in section 6.

Mathematical model

Consider the transient natural convection and mass transfer flow of viscous reactive, incompressible and electrically conducting fluid under the influence of a transversely magnetic field of strength B_0, in a vertical channel formed by two infinite vertical parallel plates separated by a distance H as shown in Fig. 1. Since the plates are of infinite length, the flow is assumed to be laminar and fully developed. The magnetic Reynolds number is assumed to be small so that the induced magnetic field and the hall effects of MHD are negligible. At time $t' \le 0$, both the fluid and the plates are at rest and at same temperature and concentration $T_0^{'}$ and $C_0^{'}$ respectively. At $t' > 0$ the temperature and concentration of the plate $y' = 0$ is raised to $T_\omega^{'}$ and $C_\omega^{'}$, and thereafter remains constant and that of $y' = H$ is lowered to $T_0^{'}$ and $C_0^{'}$, where $T_\omega^{'} > T_0^{'}$ and $C_\omega^{'} > C_0^{'}$. All the physical properties are assumed to be constant excluding density in the buoyancy term. Following Jha e*t al*. (2011a, 2011b, 2012 and 2013) and neglecting the reacting viscous fluid consumption, the governing equations under the Boussinesq's approximation can be written as

ISSN: 1597 – 9928 Science and Education Development Inst., Nigeria

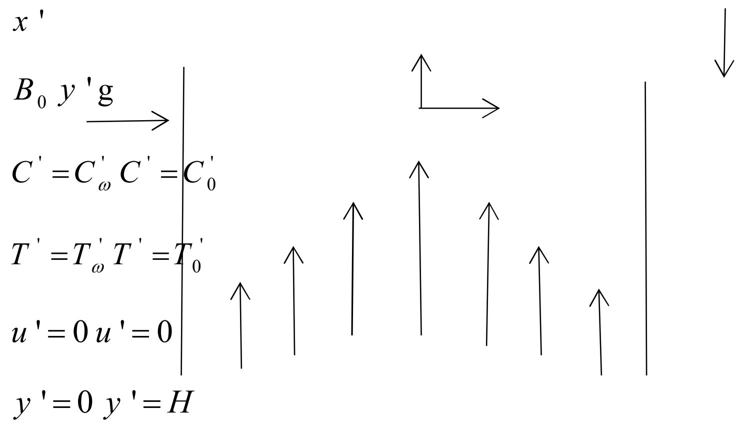

Fig.1. Schematic diagram of the physical model and coordinate system

$$\frac{\partial u'}{\partial t'} = \nu \frac{\partial^2 u'}{\partial y'^2} + g\beta(T' - T_0') + g\beta^*(T' - T_0') - \frac{\sigma B_0^2 u'}{\rho} \tag{1}$$

$$\frac{\partial C'}{\partial t'} = D_m \frac{\partial^2 C'}{\partial y'^2} + \frac{D_m k_T}{T_m}\frac{\partial^2 T'}{\partial y'^2} \tag{2}$$

$$\frac{\partial T'}{\partial t'} = \frac{k}{\rho C_p}\frac{\partial^2 T'}{\partial y'^2} + \frac{Q C_0^* A}{\rho C_p} e^{\left(\frac{-E}{RT'}\right)} \tag{3}$$

The initial and boundary conditions for the present problem are

$$\left.\begin{array}{l} t' \le 0 : u' = 0,\ T' \to T'_0,\ C' \to C'_0,\ 0 \le y' \le H \\ t' > 0 : u' = 0, T' = T_\omega',\ C' = C_\omega' \quad at \qquad y' = 0 \\ \qquad u' = 0,\ T' = T_0',\ C' = C_0' \quad as \qquad y' \to H \end{array}\right\} \tag{4}$$

Where σ is the conductivity of the fluid, B_0 is the electromagnetic induction, β is the coefficient of thermal expansion, β^* is the coefficient of concentration expansion, Q is the heat of reaction, A is the rate constant, E is the activation energy, R is the universal gas constant, ν is the kinematic viscosity, C_0^* is the initial concentration of the reactant species, g is the gravitational force, C_p is the specific heat at constant pressure, k is the thermal conductivity of the fluid, ρ is the density of the fluid, D_m is the coefficient of mass diffusivity, T_m is the mean fluid temperature, and k_T is the thermal diffusion ratio.

ISSN: 1597 – 9928 Science and Education Development Inst., Nigeria

In order to solve equations (1) to (4), we employ the following dimensionless parameters

$$\left.\begin{array}{l} y=\frac{y'}{H},\ t=\frac{t'\nu}{H^2},\ u=\frac{u'}{\nu_0},\quad \Pr=\frac{\nu\rho C_p}{k},\quad Gc=\frac{g\beta^* RC_0^2H^2}{E\nu\nu_0}, Gr=\frac{g\beta RT_0^2H^2}{E\nu\nu_0} \\ \theta=\frac{E(T'-T_0)}{RT_0^2}, \lambda=\frac{QC_0AEH^2}{RT_0^2}e^{\left(\frac{-E}{RT_0}\right)},\ Sc=\frac{\nu}{D_m},\quad Sr=\frac{k_TT_0^2}{T_mC_0^2}, C=\frac{E(C'-C_0)}{RC_0^2} \\ \varepsilon=\frac{RT_0}{E},\ \theta_T=\frac{E(T_\omega-T_0)}{RT_0^2}, C_T=\frac{E(C_\omega-C_0)}{RC_0^2},\quad M=\frac{\sigma B_0^2H^2}{\nu\rho} \end{array}\right\} \tag{5}$$

Using (5), the equations (1) to (4) can take the following form:

$$\frac{\partial u}{\partial t}=\frac{\partial^2 u}{\partial y^2}+Gr\theta+GcC-Mu \tag{6}$$

$$Sc\frac{\partial C}{\partial t}=\frac{\partial^2 C}{\partial y^2}+Sr\frac{\partial^2\theta}{\partial y^2} \tag{7}$$

$$\Pr\frac{\partial\theta}{\partial t}=\frac{\partial^2\theta}{\partial y^2}+\lambda e^{\left(\frac{\theta}{1+\varepsilon\theta}\right)} \tag{8}$$

The initial and boundary conditions in dimensionless form are

$$\left.\begin{array}{l} \quad u=0,\ \theta=0,\quad 0\le y\le 1, t\le 0 \\ t>0: u=0,\ \theta=\theta_T, C=C_T\ \ at\ \ y=0 \\ \quad u=0, \theta=0,\ C=0,\ \ as\ \ y=1 \end{array}\right\} \tag{9}$$

Analytical solutions

The governing equations (8) presented in the previous section are highly nonlinear and exhibit no analytic solutions. The analytical solutions have played significant role in validating and exploring computer routines of complicated problems. We reduce the governing equations of this problem into a form that can be solved analytically by setting $\partial u/\partial t=0$, $\partial\theta/\partial t=0$ and $\partial C/\partial t=0$ to obtain the steady state version of the problem. The steady state solutions of (6) to (8) with the help of (9), using perturbation series method of the form

$$\left.\begin{array}{l} u=u_0+\lambda u_1+\lambda^2u_2 \\ C=C_0+\lambda C_1+\lambda^2C_2 \\ \theta=\theta_0+\lambda\theta_1+\lambda^2\theta_2 \end{array}\right\} \tag{10}$$

ISSN: 1597 – 9928 Science and Education Development Inst., Nigeria

for velocity, concentration and temperature respectively by taking $\theta_T = 1$ and $C_T = 1$ at the boundary can be written as

$$u=\left[A\cosh(\sqrt{M}y)+B\sinh(\sqrt{M}y)+H_1y+H_2\right]+\left[D_1\cosh(\sqrt{M}y)+D_2\sinh(\sqrt{M}y)+H_3y^4+H_4y^3+H_5y^2+H_6y+H_7\right]+$$
$$\left[D_3\cosh(\sqrt{M}y)+D_4\sinh(\sqrt{M}y)+H_8y^7+H_9y^6+H_{10}y^5+H_{11}y^4+H_{12}y^3+H_{13}y^2+H_{14}y+H_{15}\right] \quad (11)$$

$$C=(1-y)+\lambda\left[k_3y-\frac{Sr(a-2)}{2}y^2-\frac{Sr(1-2a)}{6}y^3-\frac{Sra}{12}y^4\right]+\lambda^2\left[k_4y+\frac{Srk_1y^4}{12}+\frac{Sr(a-2)}{40}y^5+\frac{Sr(1-2a)}{180}y^6+\frac{Sra}{504}y^7\right] \quad (12)$$

$$\theta=(1-y)+\lambda\left[k_1y+\frac{(a-2)}{2}y^2+\frac{(1-2a)}{6}y^3+\frac{a}{12}y^4\right]+\lambda^2\left[k_2y-\frac{k_1y^4}{12}-\frac{(a-2)}{40}y^5-\frac{(1-2a)}{180}y^6-\frac{a}{504}y^7\right] \quad (13)$$

Using equations (11) to (13), we write the steady state skin friction, Sherwood number and Nusselt number on the boundaries as

$$\left.\frac{\partial u}{\partial y}\right|_{y=0}=\left[B\sqrt{M}+H_1\right]+\lambda\left[D_1\sqrt{M}+H_6\right]+\lambda^2\left[D_2\sqrt{M}+H_{14}\right] \quad (14)$$

$$\left.\frac{\partial u}{\partial y}\right|_{y=1}=\left[-A\sqrt{M}\sinh(\sqrt{M})+B\sqrt{M}\cosh(\sqrt{M})+H_1\right]+\lambda\left[-D_1\sqrt{M}\sinh(\sqrt{M})+D_2\sqrt{M}\cosh(\sqrt{M})+4H_3+3H_4+2H_5+H_6\right]+$$
$$\lambda^2\left[-D_3\sqrt{M}\sinh(\sqrt{M})+D_4\sqrt{M}\cosh(\sqrt{M})+7H_8+6H_9+5H_{10}+4H_{11}+3H_{12}+2H_{13}+H_{14}\right] \quad (15)$$

$$-\left.\frac{\partial C}{\partial y}\right|_{y=0}=-\left(-1+\lambda k_3+\lambda^2k_4\right) \quad (16)$$

$$\left.\frac{\partial C}{\partial y}\right|_{y=1}=-1+\lambda\left[k_3-Sr(a-2)-\frac{Sr(1-2a)}{2}-\frac{Sra}{3}\right]+\lambda^2\left[k_4+\frac{Srk_1}{3}+\frac{Sr(a-2)}{8}+\frac{Sr(1-2a)}{30}+\frac{Sra}{72}\right] \quad (17$$

$$-\left.\frac{\partial \theta}{\partial y}\right|_{y=0}=-\left(-1+\lambda k_1+\lambda^2k_2\right) \quad (18)$$

$$\left.\frac{\partial \theta}{\partial y}\right|_{y=1}=-1+\lambda\left[k_1+(a-2)+\frac{(1-2a)}{2}+\frac{a}{3}\right]+\lambda^2\left[k_2-\frac{k_1}{3}-\frac{(a-2)}{8}-\frac{(1-2a)}{30}-\frac{a}{72}\right] \quad (19)$$

The constants A, B, $H_1, H_2,\ H_3,\ H_4, H_5, H_6, H_7, H_8, H_9, H_{10}, H_{11}, H_{12}, H_{13}, H_{14}, H_{15}, D_1, D_2, D_3,$ $D_4, a\ , k_1, k_2, k_3, k_4$ are defined in the appendix section.

Numerical solutions

The set of partial differential equations (6) to (8) with the boundary conditions (9) are solved numerically using semi-implicit finite difference scheme given by (Makinde and

ISSN: 1597 – 9928 Science and Education Development Inst., Nigeria

Chinyoka, 2011). We used forward difference formulas for all time derivatives and approximate both the second and first derivatives with second order central differences. The semi-implicit finite difference equation corresponding to equations (6) to (8) are as follows

$$-r_1 u_{j-1}^{(N+1)} + (1+2r_1)u_j^{(N+1)} - r_1 u_{j+1}^{(N+1)} = r_2 u_{j-1}^{(N)} + (1-2r_2 - M\,\Delta t)u_j^{(N)} + r_2 u_{j+1}^{(N)} + \Delta t Gr\,\theta_j^N + \Delta t Gc C_j^N \tag{20}$$

$$-r_1 C_{j-1}^{(N+1)} + (Sc+2r_1)C_j^{(N+1)} - r_1 C_{j+1}^{(N+1)} = r_2 C_{j-1}^{(N)} + (Sc-2r_2)C_j^{(N)} + r_2 C_{j+1}^{(N)} + r_3\left(\theta_{j-1}^N - 2\theta_j^N + \theta_{j+1}^N\right) \tag{21}$$

$$-r_1\theta_{j-1}^{(N+1)} + (\Pr+2r_1)\theta_j^{(N+1)} - r_1\theta_{j+1}^{(N+1)} = r_2\theta_{j-1}^{(N)} + (\Pr-2r_2)\theta_j^{(N)} + r_2\theta_{j+1}^{(N)} + \lambda\Delta t\exp\left(\frac{\theta_j^{(N)}}{1+\varepsilon\theta_j^{(N)}}\right) \tag{22}$$

Where $r_1 = \xi\Delta t/\Delta y^2$, $r_2 = (1-\xi)\Delta t/\Delta y^2$, $r_3 = Sr\,\Delta t/\Delta y^2$ and $0 \le \xi \le 1$. We chose $\xi = 1$ the detailed reasons to this particular selection is documented by (Makinde and Chinyoka, 2011). Also the analytical solutions displayed in the previous section are used as a check on the accuracy and effectiveness of the numerical scheme. Again, in order to reconfirm the accuracy of the scheme, the numerical results for velocity, concentration and temperature are compared with the analytical solutions. It has been found that the numerical values of the velocity, concentration and temperature fields calculated from the expressions (11) to (13) have matched very well with the numerical obtained from the expressions (20) to (22) at the steady state time. See fig.2 for the graph of the numerical solutions at steady state and steady-state analytical solutions for velocity, concentration and temperature fields

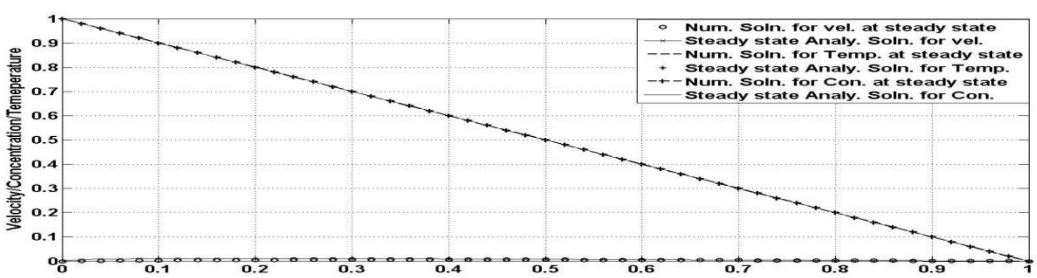

Fig 2. Unsteady and steady state solutions for velocity, concentration and temperature profiles

ISSN: 1597 – 9928 Science and Education Development Inst., Nigeria

Results and Discussion

To study the behavior of the solutions, numerical calculations for some values of Frank-Kamenetskii parameter (λ), Soret number (Sr), magnetic parameter (M), Schmidt number (Sc), Prandtl number (Pr), thermal Grashof number (Gr), mass Grashof number (Gc), and non-dimensional time (t) have been carried out. Unless otherwise stated, the values: $\lambda = 0.1$, $Gr = 0.1$, M =1, $Gc = 0.1$, Sr = 0.1 , $\theta_T = 1$, $C_T = 1$, Pr = 0.71, Sc = 0.62, and $\varepsilon = 0.01$ are used for the investigation. Results obtained are displayed graphically for velocity, temperature, concentration, skin friction, Nusselt number and Sherwood number for various flow parameters.

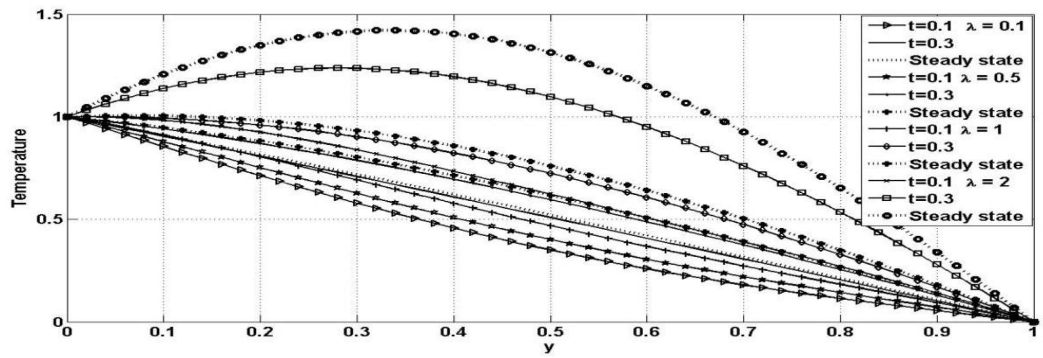

Fig.3. Variation of unsteady and steady state temperature for λ and t

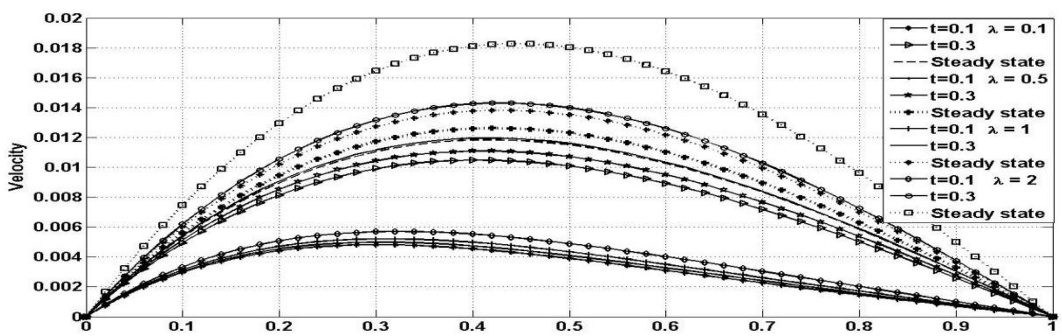

Fig.4. Variation of unsteady and steady state velocity for λ and t

ISSN: 1597 – 9928 Science and Education Development Inst., Nigeria

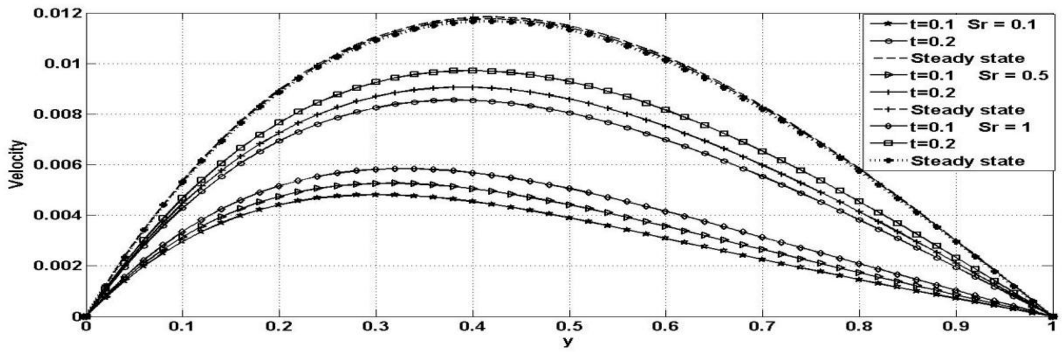

Fig.5. Variation of unsteady and steady state velocity for Sr and t

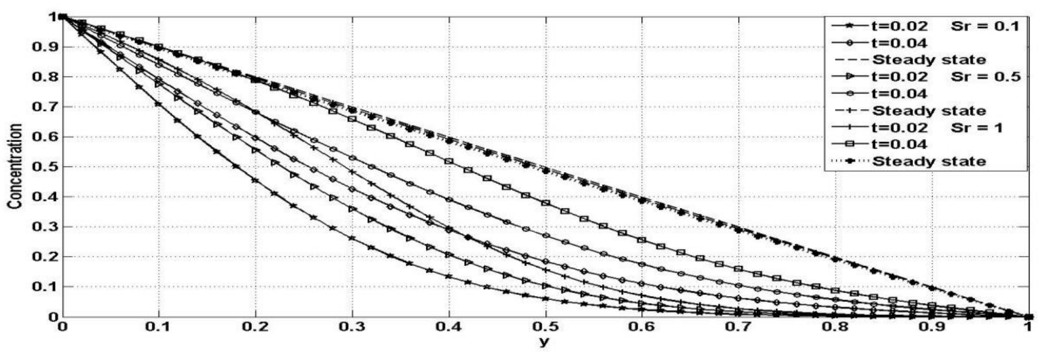

Fig.6. Variation of unsteady and steady state concentration for Sr and t

Figs 3 and 4 show unsteady as well as steady state temperature and velocity profiles for different values of the reaction parameter λ and non-dimensional time. It is observed from these figures that the temperature and velocity increases with increase in non-dimensional time until a steady state condition is attained. From Fig 3 it is seen that as λ increases, both unsteady and steady-state temperature increases. This is physically true since an increase in λ lead to significant increases in the reaction and viscous heating source terms and hence significantly increases the fluid temperature. The significant temperature rise in response to the increased λ lead to the increases in the fluid velocity sees (Fig 4) Also, Fig 4 reveals that for small value of λ and time, their effect on the unsteady velocity is insignificant. The effects of the Soret number Sr and non-dimensional time on the velocity and concentration profiles is illustrated in Figs.5 and 6 respectively. It is evident from these figures that increasing values of Sr increases both velocity and concentration of the fluid. We can also figure that mass transfer rate is strongly influenced by Soret effect. It is noted from Figs.5 and 6 that as time increases, unsteady state velocity and concentration increases, while at steady state both velocity and concentration of the fluid slightly decreases. In other words,

ISSN: 1597 – 9928 **Science and Education Development Inst., Nigeria**

larger time decreases both fluid velocity and concentration of the fluid in the presence of higher values of Sr.

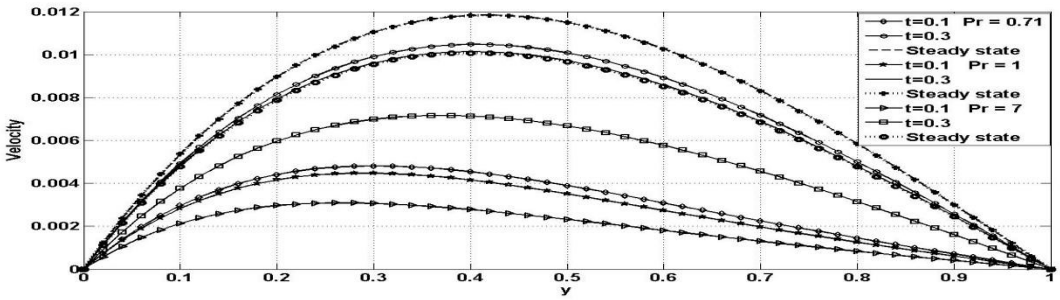

Fig.7. Variation of unsteady and steady state velocity for Pr and *t*

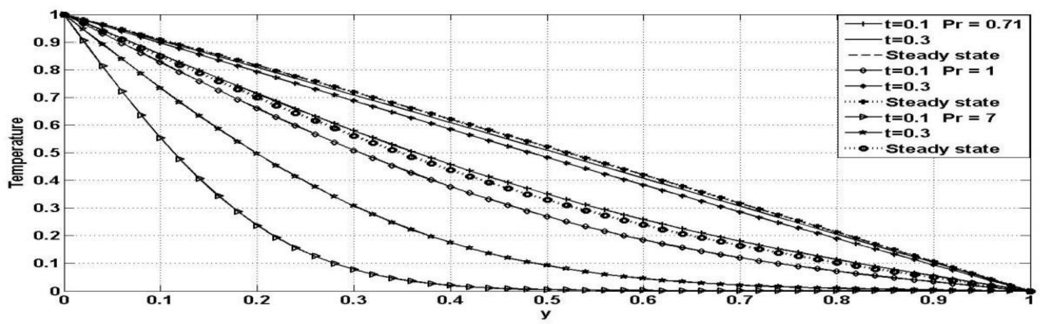

Fig.8. Variation of unsteady and steady state temperature for Pr and *t*

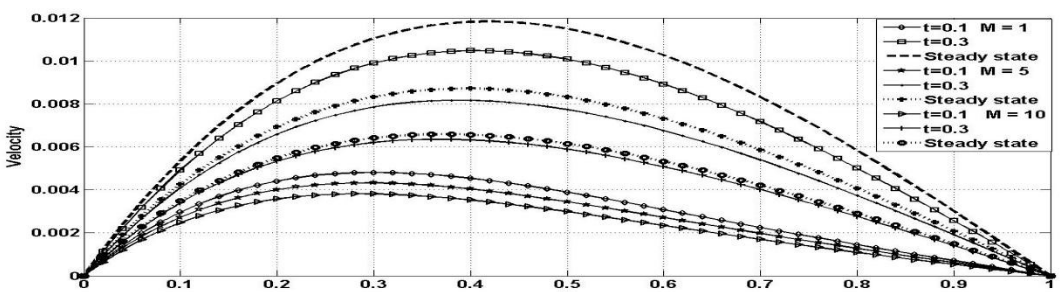

Fig.9. Variation of unsteady and steady state velocity for M and *t*

The effects of the Prandtl number and time on the velocity and temperature fields is depicted in Figs 7and 8 respectively. From these Figures it is observed that both velocity and temperature of the fluid decreases with increasing values of Pr. Larger values of the Prandtl number correspondingly decrease the strength of the source terms in the temperature equation and hence in turn reduce the over-all temperature as clearly illustrated in Fig 8. The reduced temperature results in decreased fluid viscosity and hence reduced fluid velocity as can be seen in Fig7. Also Fig 7 reveals

ISSN: 1597 – 9928 Science and Education Development Inst., Nigeria

that as time increases, unsteady state velocity increases, while at steady-state velocity of the fluid decreases when Pr is large. A similar trend is noticed in the temperature of the fluid see (Fig 8). Fig 9 displays the influence of the magnetic parameter M and time on the velocity profiles. It is clearly seen that the effect of increasing the strength of magnetic parameter is to decrease velocity profiles. This is due to the fact that transverse magnetic field produces a resistivity force (Lorentz force) similar to the drag force, which shrink the velocity. It is further noticed that as time increases, the velocity increases until a steady state is reached.

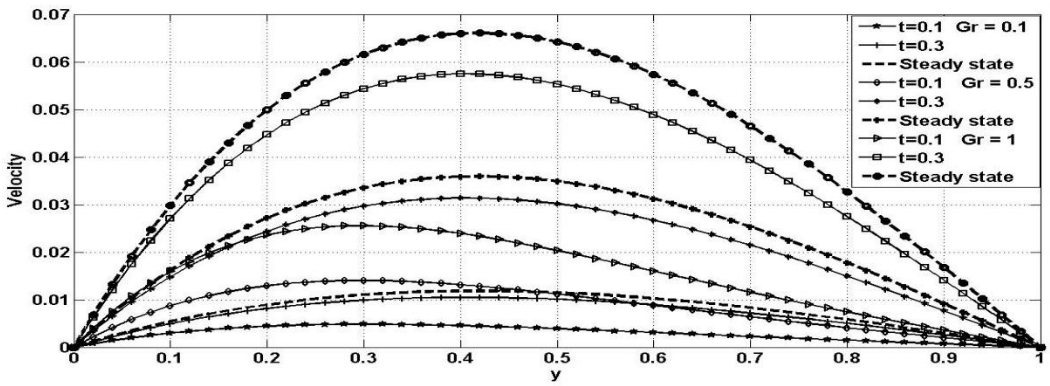

Fig.10. Variation of unsteady and steady state velocity for Gr and t

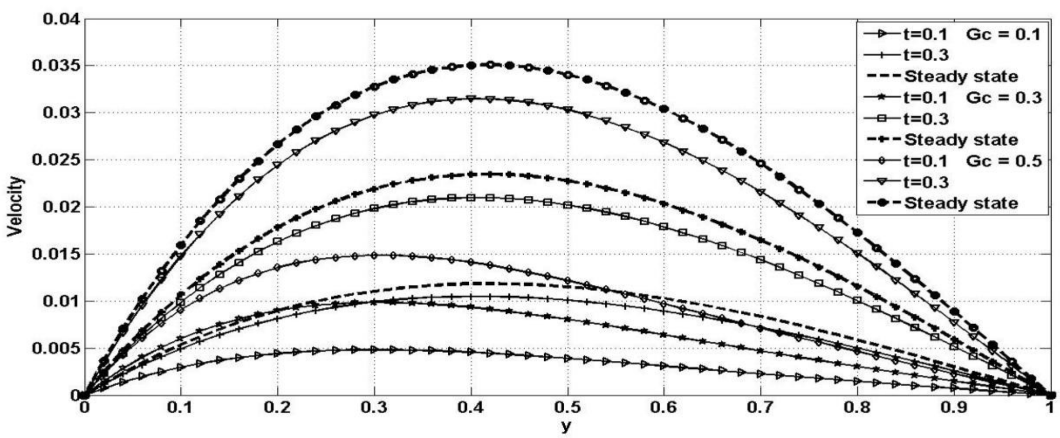

Fig.11. Variation of unsteady and steady state velocity for Gc and t

ISSN: 1597 – 9928 Science and Education Development Inst., Nigeria

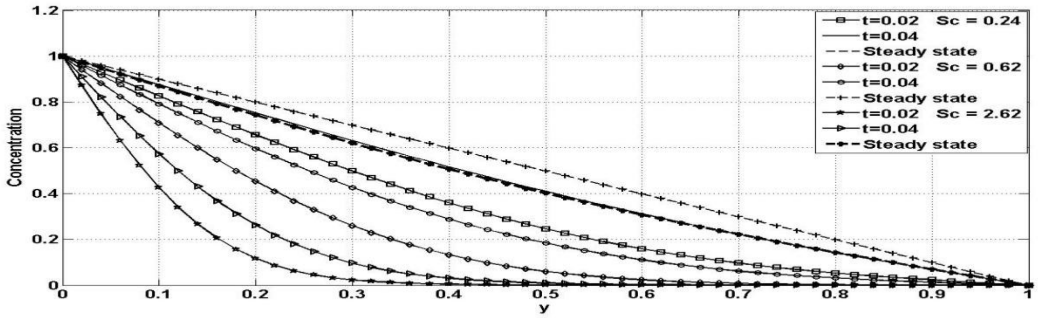

Fig 12. Variation of unsteady and steady state concentration for Sc and t

Figs 10 and 11 represent the influence of the thermal Grashof number and solutalGrashof number on the velocity profiles respectively. These plots indicate that the momentum boundary layer thickness increases with increasing values of Gr and Gc. It is evident from Fig.10 that the velocity increases with increase in the non-dimensional time. A similar trend is seen in Fig 11. Fig 12 represents the graph of concentration profile for different values of the Schmidt number and time. It is seen that the concentration distribution in the boundary layer decreases with increasing values of Sc. Also as time increases, unsteady state concentration increases, while concentration of the fluid decreases at steady state when Sc is large.

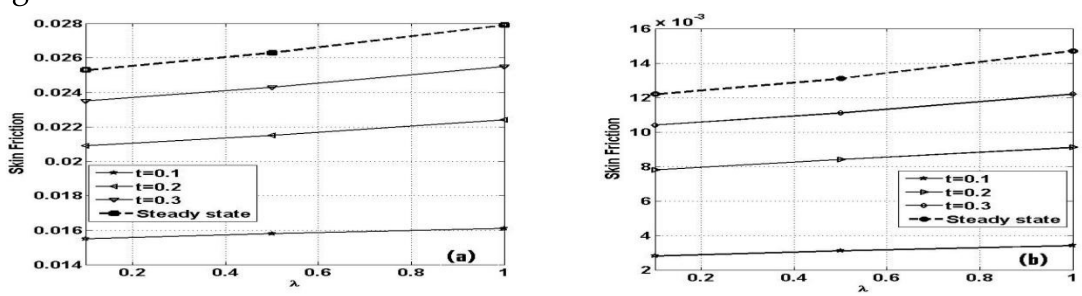

Fig.13. Variation of unsteady and steady state skin friction at $y = 0$ and $y = 1$ for λ and t

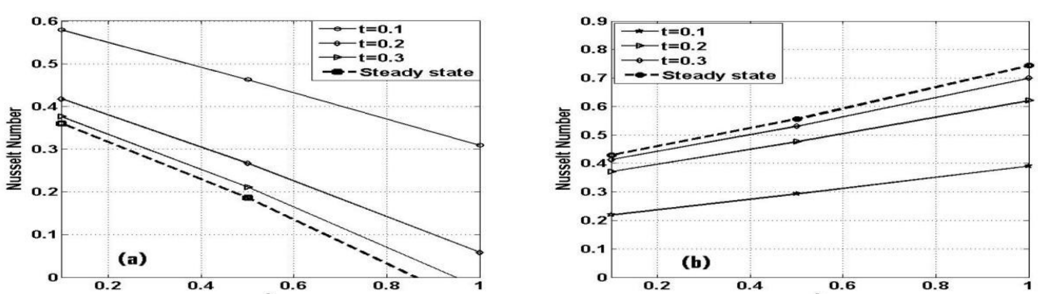

Fig.14. Variation of unsteady and steady state Nusselt number at $y = 0$ and $y = 1$ for λ and t

ISSN: 1597 – 9928 Science and Education Development Inst., Nigeria

The wall shear stress dependence on λ is illustrated in Fig13 for varying values of non-dimensional time at the plates $y = 0$ and $y = 1$ respectively. From Fig13 it can be noticed that the skin friction increases with increasing both non-dimensional time and λ at the plate $y = 0$ and $y = 1$ until a steady-state condition is achieved. Fig 14 is plotted to see the effects of time and λ on the rate of heat transfer in terms of Nusselt number at the plate $y = 0$ and $y = 1$ respectively. Fig14b reveals that the rate of heat transfer at the plate $y = 1$ increases as time and λ increases until a steady state is attained. In Fig14a the rate of heat transfer at the plate $y = 0$ decreases with increasing time and λ.

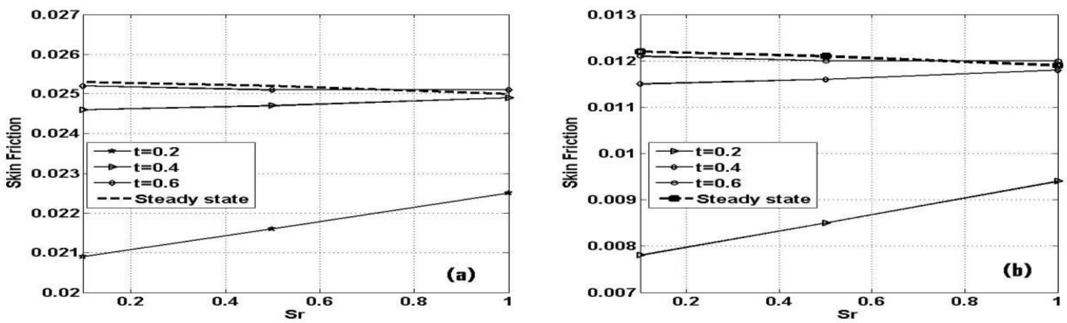

Fig.15. Variation of unsteady and steady state skin friction for Sr and t

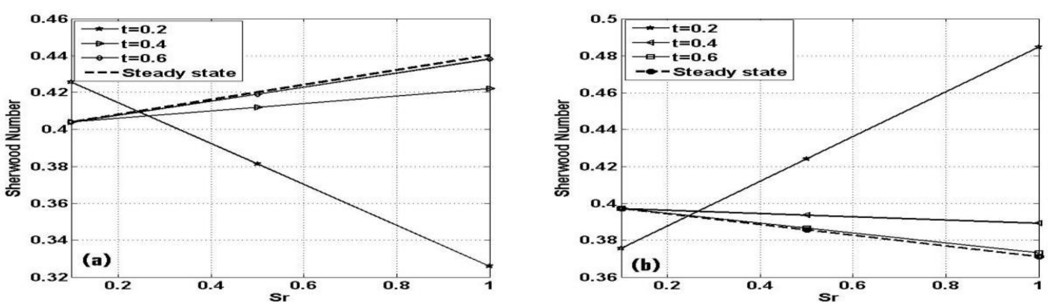

Fig.16. Variation of unsteady and steady state Sherwood number for Sr and t

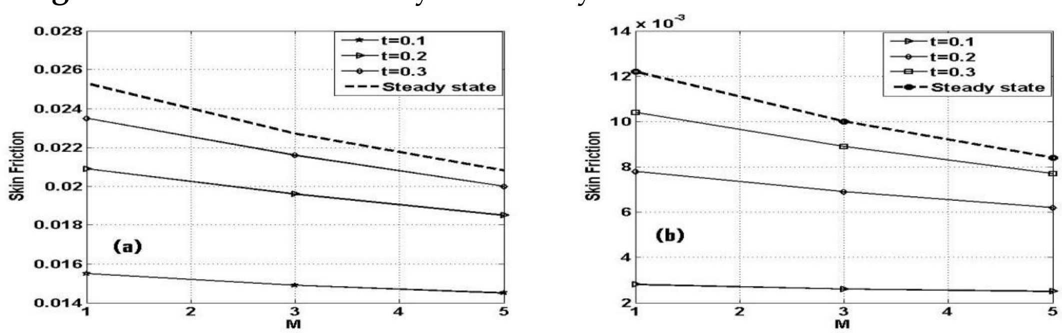

Fig.17. Variation of unsteady and steady state skin friction for M and t

ISSN: 1597 – 9928 Science and Education Development Inst., Nigeria

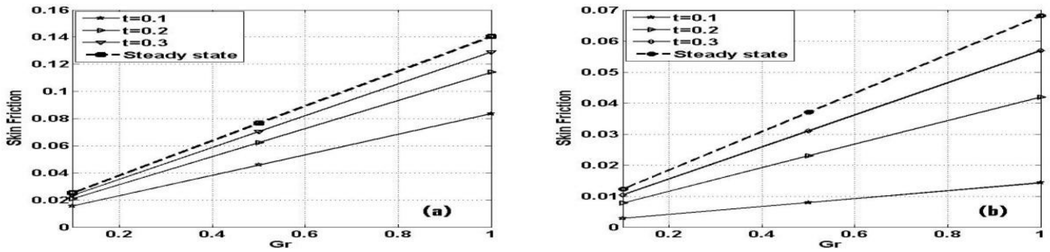

Fig.18. Variation of unsteady and steady state skin friction for Gr and t

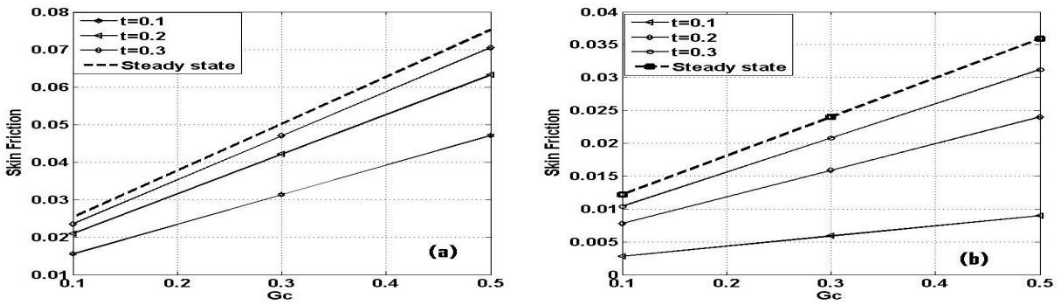

Fig.19. Variation of unsteady and steady state skin friction for Gc and t

Fig 15 shows the wall shear stress dependence on Sr for varying values of the non-dimensional time at the plates $y = 0$ and $y = 1$ respectively. From this figure it is clear that the skin friction increases as Sr increases. It is also observed that the skin friction increases with increasing time until a steady-state condition is reached. A slide decrease of the skin friction is noticed at the steady state at both plate $y = 0$ and $y = 1$ when Sr is large. Fig.16 represents the influence of Sr and time on the Sherwood number. It is reflected from Fig.16a that the Sherwood number increases with increasing Sr and time. A reverse effect is observed at the plate $y = 1$ (Fig16b). Figs 17-19 show the wall shear stress at the plate $y = 0$ and $y = 1$ for different values of magnetic parameter, thermal Grashof number, solutalGrashof number and non-dimensional time respectively. From these figures it is seen that as time increases, the frictional force due to the motion of the fluid also increases until a steady state condition is attained. From Fig17 it is evident that values of M reduce the skin friction. Figs 18 and 19 reflected that values of Gr and Gc accelerate the skin friction.

Conclusion

The problem of unsteady as well as steady hydromagnetic flow of viscous reactive fluid in the presence of transverse magnetic field and Soret effect was investigated. The velocity, concentration and temperature of the fluid for steady-state version of

ISSN: 1597 – 9928 Science and Education Development Inst., Nigeria

the problem are obtained using perturbation series method, while the complete forms of the problem are solved numerically using unconditionally and convergent semi-implicit finite difference scheme. A brief summary of the major findings is given below

(i) During the numerical analysis, an excellent agreement is found between the steady-state solutions and unsteady state solutions at large value of time
(ii) Increasing the reaction strength, Soret number, thermal Grashof number and solutalGrashof number increases the flow velocity in the momentum boundary layer, while higher values of Prandtl number and magnetic parameter decreases the flow velocity.
(iii) Increasing the reaction strength increases the temperature of the fluid, while higher values of Prandtl number reduce the temperature of the fluid.
(iv) Soret effect is to increase concentration of the fluid, while Schmidt number decreases the concentration of the fluid.

References

Campbell, A.C., Cardoso, S.S.S., and Hayhurst, A.N, (2007), A comparison of measured temperatures with those calculated numerically and analytically for an exothermic chemical reaction inside a spherical batch reactor with natural convection. *Chemical Engineering Science*, **62**, 3068-3082.

Dursunkaya, Z., Worek, W.M. (1992), Diffusion-thermo and thermal diffusion effects in transient and steady natural convection from vertical surface, *International Journal of Heat and Mass Transfer*,**35**, 2060-2065.

Emmanuel, O., Side, J., and Harris, R., (2008),Thermal diffusion and diffusion-thermo effects on combined heat and mass transfer of a steady MHD convective and slip flow due to a rotating disk with viscous dissipation and ohmic heating, *International Communications in Heat and Mass Transfer*, **35**, 908-915.

Jha, B.K., Samaila, A.K., and Ajibade, A.O., (2011a), Transient free convection flow of reactive viscous fluid in a vertical channel. *International Communications in Heat and Mass Transfer*, **38**, 633-637.

Jha, B.K., Samaila, A.K. and Ajibade, A.O., (2011b), Transient free convection flow of reactive viscous fluid in a vertical tube. *Mathematics and Computer Modelling*, **54**, 2880-2888

ISSN: 1597 – 9928 Science and Education Development Inst., Nigeria

Jha, B.K., Samaila, A.K. and Ajibade, A.O., (2012), Unsteady/steady free convection couette flow of reactive viscous fluid in a vertical channel formed by two vertical porous plate. *ISRN Thermodynamics*, **2012**, 1-10.

Jha, B.K., Samaila, A.K. and Ajibade, A.O., (2013), Unsteady natural convection couette flow of a reactive viscous fluid in a vertical channel. *Computational Mathematics and Modeling*, **24**, 432-442.

Joshi, H.M. (1988) Transient effects in natural convection cooling of vertical parallel plates, *International Communication in Heat and Mass Transfer*, **15**, 227-238.

Hartmann, J. (1937). Hydrodynamics I: Theory of the laminar flow of an electrically conducting liquid in a homogeneous magnetic field, *Kgl. Dans. Vide. Selskab.Math. Fys Med*, **14**, 1-27.

Lee, K.T., (1999), Natural convection heat and mass transfer in partially heated vertical parallel plates. *International Journal of Heat and Mass Transfer*, **42**, 4417-4425.

Makinde, O.D. and Chinyoka, T., (2011), Numerical study of unsteady hydromagnetic generalized Couette flow of a reactive third-grade fluid with asymmetric convective cooling, *Computers and Mathematics with Application*, **61**, 1167-1179.

Minto, B.J., Ingham, D.B. and Pop, I., (1998), Free convection driven by an exothermic reaction on a vertical surface embedded in porous media, *International Journal of Heat and Mass Transfer*, **41**, 11-23.

Nelson, D.J. and Wood, B.D., (1989), Combined heat and mass transfer natural convection between vertical parallel plates, *International Journal of Heat and Mass Transfer*, **32** ,1779-1787.

Postelnicu, A., (2004), Influence of a magnetic field on heat and mass transfer by natural convection from vertical surfaces in porous media considering Soret and Dufour effects, *International Journal of Heat and Mass Transfer*, **47**, 1467-1472.

Soundalgekar, V.M., and Warve, P.D., (1977), Unsteady free convection flow past an infinite vertical plate with constant suction and mass transfer, *International Journal of Heat and Mass Transfer*, **20**, 1363-1373.

ISSN: 1597 – 9928 **Science and Education Development Inst., Nigeria**

Soundalgekar, V.M. and Ganesan, P., (1981), Finite difference analysis of transient free convection with mass transfer on an isothermal vertical flat plate, *International Journal of Engineering Science*, **19**, 757-770.

Tsai, R. and Huang, J.S., (2009), Numerical study of Soret and Dufour effects on heat and mass transfer from natural convection from over a vertical porous medium with variable wall heat fluxes, *Computational Materials Science*, **47**, 23-30.

Turkyilmazoglu, M. and Pop, I. (2012), Soret and heat source effects on the unsteady radiative MHD free convection flow from an impulsively started infinite vertical plate, *International Journal of Heat and Mass Transfer*, **55**, 7635-7644.

Yan, W.M. and Lin, T.F., (1990), Combined heat and mass transfer in natural convection between vertical parallel plates with film evaporation, *International Journal of Heat and Mass Transfer*, **33**, 529-541.

Appendix

$$a=\varepsilon-1/2,\ k_1=-\frac{(a-2)}{2}-\frac{(1-2a)}{6}-\frac{a}{12},\ k_2=\frac{k_1}{12}+\frac{(a-2)}{40}+\frac{(1-2a)}{180}+\frac{a}{504},\ H_1=-\frac{(Gr+Gc)}{M}$$

$$k_3=\frac{Sr(a-2)}{2}+\frac{Sr(1-2a)}{6}+\frac{Sra}{12},\ k_4=-\frac{Srk_1}{12}-\frac{Sr(a-2)}{40}-\frac{Sr(1-2a)}{180}-\frac{Sra}{504},\ H_2=\frac{(Gr+Gc)}{M},$$

$$A=-H_2,\ B=\frac{H_2\cosh(\sqrt{M})}{\sinh(\sqrt{M})}-\frac{(H_1+H_2)}{\sinh(\sqrt{M})},\ H_3=-\frac{(GcSr-Gr)a}{12M},\ H_4=-\frac{(GcSr-Gr)(1-2a)}{6M},$$

$$H_5=\frac{12H_3}{M}-\frac{(GcSr-Gr)(a-2)}{2M},\ H_6=\frac{(Grk_1+Gck_3)+6H_4}{M},\ H_7=\frac{2H_5}{M},\ D_1=-H_7,$$

$$D_2=\frac{H_7\cosh(\sqrt{M})}{\sinh(\sqrt{M})}-\frac{(H_3+H_4+H_5+H_6+H_7)}{\sinh(\sqrt{M})},\ H_8=-\frac{(Gr-GcSr)a}{504M},\ H_9=-\frac{(Gr-GcSr)(1-2a)}{180M},$$

$$H_{10}=\frac{42H_8}{M}-\frac{(Gr-GcSr)(a-2)}{40M},\ H_{11}=\frac{30H_9}{M}-\frac{(Gr-GcSr)k_1}{12M},$$

$$H_{12}=\frac{20H_{10}}{M},\ H_{13}=\frac{12H_{11}}{M},,\ H_{14}=\frac{6H_{12}}{M}-\frac{(Grk_2+Gck_4)}{M},\ H_{15}=\frac{2H_{13}}{M},\ D_3=-H_{15},$$

$$D_4=\frac{H_{15}\cosh(\sqrt{M})}{\sinh(\sqrt{M})}-\frac{(H_8+H_9+H_{10}+H_{11}+H_{12}+H_{13}+H_{14}+H_{15})}{\sinh(\sqrt{M})}$$

ISSN: 1597 – 9928 Science and Education Development Inst., Nigeria